Published in the Proceedings of the 16th International Aluminum Alloys Conference (ICAA16) 2018
ISBN: 978-1-926872-41-4
by the Canadian Institute of Mining, Metallurgy & Petroleum

A METHODOLOGY TO ASSESS THE SPATIAL DISTRIBUTION OF DISPERSOIDS IN Al-Mg-Si ALLOYS

M.S. Remøe, I. Westermann and *K. Marthinsen

Department of Materials Science and Engineering, Norwegian University of Science and Technology, NO-7491 Trondheim, Norway
*(*Corresponding author: knut.marthinsen@ntnu.no)*

ABSTRACT

Al-Mg-Si alloys often add small additions of e.g. Mn or Cr, to form dispersoids, which may act as nucleation sites for Mg_2Si particles after homogenization. The purpose is to ensure a high density of uniformly distributed small β'-particles, which can be dissolved during further processing prior to the final age hardening step. However, their density and spatial distribution are critically dependent on the homogenization procedure. It is therefore important to have a robust and reliable method for assessing their spatial distribution. In the present work an existing methodology for assessing spatial uniformity, the Global Shannon Entropy (GSE), has been implemented and evaluated for different dispersoid structures characterized by scanning electron microscopy. This metric is highly dependent on the parameters used, but by careful selection of adequate parameters, it can be effective in detecting non-uniformity. An important weakness with the GSE was identified, and a modification to improve on the ability to differentiate degrees of non-uniformity is suggested. To evaluate the proposed methodology, the effect of heating rate on dispersoid precipitation behaviour during homogenisation of four Al-Mg-Si alloys with different Mn/Cr-content has been investigated. The metric with the new term has demonstrated promising results, and improved the ability to differentiate degrees of spatial uniformity.

KEYWORDS

Al-Mg-Si, Dispersoids, Homogenisation, Spatial distribution, Global Shannon Entropy

INTRODUCTION

Al-Mg-Si series alloys are the most common aluminium extrusion alloys and are attractive for applications in a range of sectors (e.g. construction, automotive and recently also in consumer electronics), due to their generally good combination of strength, ductility and corrosion resistance. However, their extrudability and end properties depend critically on the alloy chemistry as well as prior processing conditions. Coarse β-AlFeSi or Mg_2Si-particles typically have a detrimental effect on extrudability, while small dispersoid particles may affect recrystallization, grain growth and precipitation of Mg and Si. The strengthening potential in the final age hardening step depends strongly on the amount of Mg and Si in solid solution after extrusion.

The manner in which these particles are spatially distributed will decide whether the final product will exhibit uniform properties, and the number density and sizes will determine the extent of the effect. As such, these are important characteristics.

Al-Mg-Si alloys often have alloy additions like Mn, Cr and Zr, which form dispersoids. With a relatively high level of Mn, the dispersoids act as recrystallization inhibitors, and their number density and spatial distribution will have a large influence on the final grain sizes and their uniformity. Dispersoids may also act as potent nucleation sites for β'-Mg_2Si, which leads to a higher quench sensitivity as the number density of dispersoids increases. This is generally regarded as a negative effect, as it may reduce the ageing potential after extrusion. But if the dispersoids can be used to control the precipitation of Mg and Si during cooling from homogenisation, it may improve the extrudability significantly.

During homogenisation, coarse Mg_2Si particles present after casting or precipitated during heating, dissolve as the heat treatment proceeds. However, they may re-precipitate during cooling, and reduce the extrudability of the billets (Bichel et al., 1981; Lohne & Dons, 1983). With a sufficiently slow cooling rate, Mg and Si precipitate as coarse β-Mg_2Si particles on grain boundaries in the temperature range of ~525-425°C depending on the alloy composition (Bryant et al., 1989). If these particles are sufficiently large (> 1 μm), they have been found to have a negative impact on the extrusion speed by causing local melting in the surface area of the billets, as temperature increases during the extrusion process (Reiso et al., 1995; Reiso, 2004). Moreover, if the Mg_2Si-particles are large, they will not dissolve during extrusion and, hence, the final ageing potential is reduced.

However, if the size and spatial distribution of dispersoids are carefully controlled as well as the cooling rate, the dispersoids may act as nucleation sites for smaller β'-Mg_2Si particles precipitating during cooling after homogenization (formed in the temperature range 425-250°C, if there is Mg and Si left in solid solution; Bryant and Rise, 1989). These finer β'-precipitates will dissolve as the temperature increases during extrusion allowing for higher extrusion speeds, while lowering the extrusion pressure as Mg and Si are bound to non-hardening particles, and leaving Mg and Si available for age hardening after extrusion. However, if the dispersoids are to act as nucleation agents to control the sizes of the β'-phase, it is critical to control the dispersoid density and spatial distribution. A low number density of dispersoids should result in larger β'-particles, while a higher density should yield smaller β'. As Mg and Si are fairly homogeneously distributed during homogenisation, a uniform spatial distribution of dispersoids is also essential to ensure homogeneous precipitation of β' during cooling. If an area is depleted of dispersoids, precipitation of coarse β-Mg_2Si on grain boundaries may occur in that area, and as mentioned above, such coarse particles are detrimental to the extrudability of the billet (Reiso, 2004; Sheppard, 1999).

In view of the apparent importance of the dispersoid density and spatial distribution on the precipitation behaviour of Mg_2Si-particles after homogenisation, and thus their influence on the subsequent processing and final ageing potential, it is important to be able to characterize the precipitation behaviour of dispersoids, both in terms of density and spatial distribution. An important objective of the present study has therefore been to develop a reliable procedure for the characterization of the density and spatial distribution of dispersoids in aluminium alloys. Scanning electron microscopy (SEM) has been used to characterize the dispersoid structures in different aluminium alloys and conditions, while an existing methodology for

assessing spatial uniformity, the Global Shannon Entropy (GSE), has been implemented and evaluated to assess their spatial distribution. To test and evaluate the proposed methodology, the dispersoid precipitation behaviour during different homogenisation procedures of four Al-Mg-Si alloys with different Mn/Cr-content has been investigated.

THEORY

Robust and reliable quantitative methods for assessing the spatial distribution of, e.g. particles and precipitates in the aluminium matrix have, with a few exceptions (Avrami, 1939, 1940, 1941), mainly been missing, and today the evaluation is usually done manually and qualitatively by human operators. However, recent years' interest in metal matrix nanocomposites (MMNCs) has resulted in an intensified effort in implementing mathematical models for the assessment of spatial particle distributions. In these materials, where nano-sized ceramic particles are embedded into a metal matrix, the uniformity of their distribution is critical to their performance in terms of mechanical properties (Zhou et al., 2012; Kam et al., 2013) give thorough reviews of such metrics, and compare their effectiveness in various tests. In these metrics, particles are treated as dimensionless points, and the resulting patterns are referred to as *spatial point patterns*. To provide a reference, patterns of *complete spatial randomness* (CSR) are created, and a specific pattern of interest is tested and compared to the CSR pattern to assess their uniformity (or more precisely their deviation from complete spatial randomness). The CSR patterns are thus regarded as having optimal uniformity.

There are two main ways of quantifying the uniformity of spatial point patterns, namely with quadrat-based metrics and distance-based metrics. Distance-based metrics are based on the distances between each point. However, it is pointed out by Cressie (1993) that it is arbitrary if you choose the nearest neighbour, second-nearest, third-nearest etc., and this may largely influence the results. Moreover, a problem arises when a point is located closer to the frame of the image than any other point. This is known as the "edge-effect", and several methods have been developed to account for this (Diggle, 2013).

In general, the quadrat-based metrics *index of dispersion* (ID) and *global shannon entropy* (GSE) have been found to be both more effective and convenient than the distance-based metrics, and is therefore explored further in this study, to assess the spatial distribution of dispersoids in aluminium alloys. The GSE is an entropic measure, where the probability of a point falling into a certain quadrat, p_i, is calculated for each quadrat in an image grid. The GSE is then calculated through

$$GSE = -\left[\sum_{i=1}^{q} p_i \log(p_i)\right] / \log(q); \quad p_i = x_i / \sum_{i=1}^{q} x_i \tag{1}$$

where x_i is the number of points found in quadrat i. Under perfect uniformity, p_i will be equal for all quadrats, namely $p_i=1/q$, and GSE=1. This ideal situation, however, may only occur under conditions of regularity, which rarely occur in nature. CSR patterns, which better reflect the ideal for spatial distributions such as those for dispersoids, will return a GSE lower than 1. How much lower is dependent on the parameters in use. Moreover, as non-uniformity increases, the GSE decreases until all points are found in one quadrat, and GSE=0.

In order to assess the GSE metric and its ability to differentiate spatial non-uniformity, the GSE was calculated from a sample population of 100 spatial synthetic point patterns, to be comparable with the results from backscatter scanning electron microscopy (SEM). The resolution of the generated images were also set equal to the SEM images, with an area of, $A = 23 \cdot 33$ µm. Each "*image*" was given a random number of points, based on the density chosen, n (average number of points per image). CSR patterns were generated by assigning random x- and y-coordinates to each point in a pattern, until the amount of points in each pattern, x_i, was fulfilled. To test the efficiency of the GSE metric in detecting non-uniformity, matern cluster patterns (i.e. clusters, for which the centres are randomly distributed) were chosen, as they have been found to pose the biggest challenge for the metrics properties (Zhou et al., 2012; Kam et al., 2013). Synthetic cluster patterns were constructed, with different characteristics in terms of cluster intensity n, amount of points per

cluster, n_c, and spatial distribution of points (distance from cluster center), by varying the standard deviation, σ, of the normal distribution of points within a cluster.

Due to the nature of the quadrat-based metrics, they will necessarily be dependent on the intensity of points in the patterns. The more points, the higher the metric will score for a given spatial distribution, until the value saturates at a certain intensity. Non-uniform patterns must therefore always be tested against CSR patterns with the same average density, n, as a point of reference. This reduces the "smoothing effect", making it easier to compare the spatial distribution of samples with different densities. In the current study, all patterns have been normalized in the following way:

$$GSE = GSE_{non-uniform} / GSE_{CSR} \quad (2)$$

For the optimum detection power of the metric, the value for q should correspond with the intensity of points in the image. If there is a large number of quadrats, and few points in the pattern, it will mean that a large number of quadrats will be empty. This will result in a low GSE_{CSR}, and the detection power of the metric will be reduced.

An important weakness of the GSE metric is that it does not provide enough spatial information. The lack of spatial information on the points inside each quadrat was mentioned in the introduction; however, there is also a lack of information about the order of the quadrats in the grid. For example, the two grids in Figure 1 represents very different spatial distributions, but the GSE metric cannot distinguish between them, and will in both cases result in GSE = 0.78. This is a major drawback, and likely the reason why Zhou et al. (2012) and Kam et al. (2013) found the metric to perform poorly at large q's. Intuitively, large q's should provide a higher resolution and therefore improved accuracy. In fact, ideally, using large enough q's should result in the resolution approaching that of distance-based metrics, however, GSE in its current form is not able to benefit from the larger amount of information available when using a higher resolution.

Metrics which account for the location of the quadrats in the grid are called *spatial auto-correlation measures*. Kam et al. (2013) included four such metrics for which the Local Gi (LG) had the best detection power. However, it still scored well below the *index of dispersion* (ID) and the GSE, and the question is whether instead a new term may be added to the GSE to account for this problem, to combine the best of both worlds.

2		2	
	2		2
2		2	
	2		2
2		2	
	2		2

		2	2
		2	2
		2	2
		2	2
		2	2
		2	2

Figure 1. Two spatial point patterns that the GSE parameter is not able to differentiate**.**

The new term would require the ability to determine whether quadrats with large counts are confined to certain areas in the image, and quadrats with small counts to others. A simple model of how this could be solved is described below. For high q's and under CSR conditions, the quadrats with no (or a small amount of) points will be evenly distributed. This means that as you move along the rows or columns in the grid, the value of the quadrats should increase and decrease regularly. For example, in the grid to the left in Figure 1 above, moving downwards in column 1, the quadrat value will first decrease from 2 to 0, then increase to 2, before it decreases to 0 again, and so on. If there is non-uniformity, the amount of times an increase or a decrease occurs, should be lower than for CSR, as can be seen in the grid to the right in Figure 1.

In the present work, it is suggested that the GSE metric can be improved by including the amount of times the mean is crossed for each row and column in the grid. The new term would thus be the counts of crossings of the mean for a non-uniform pattern, $c\tilde{x}_{non-uniform}$ normalized to that of the CSR, $c\tilde{x}_{CSR}$. A modified GSE could then be described by

$$GSE^* = GSE \cdot c\tilde{x} = \frac{GSE_{non-uniform}}{GSE_{CSR}} \cdot \frac{c\tilde{x}_{non-uniform}}{c\tilde{x}_{CSR}} \tag{3}$$

It is necessary to point out that this approach will fail if the spatial distribution approaches uniformity. In such a case, the graph would have a very low amount of crossings, or even none, as it would rest on (or close to) the mean. However, as was mentioned earlier, regularity rarely occurs in nature, and this should not be an issue when dealing with dispersoid distributions. Under CSR, as illustrated in Figure 2, the number of crossings increases with the intensity of points in the pattern, until it saturates at approximately half of the maximum amount of crossings possible. That is, for q = 8 · 6 = 48, the maximum amount of crossings is $c\tilde{x}_{CSR}^{max} = 7 \cdot 6 + 5 \cdot 8 = 82$. Thus the number of crossings for q = 48 saturates at 41, as seen in Figure 2, and this behaviour is the same for all values of q. It is also noted that there are drops in each graph, and the drop seems to occur when the intensity of points is equal to an integer multiplied by q ($N \cdot q = n$, or n/q=1,2,3…). This may be related to an effect of regularity as it then would be possible for every square to be occupied by N points, which could result in a low number of crossings.

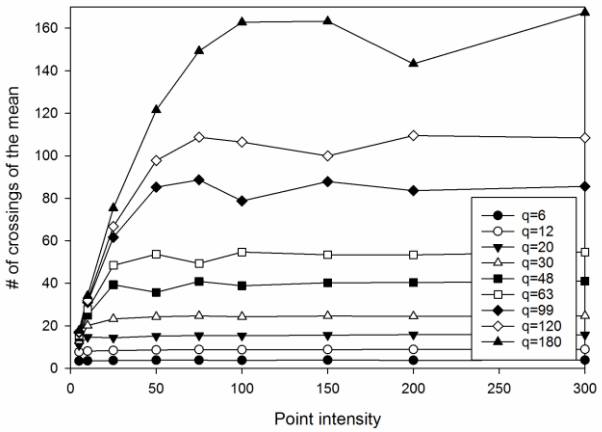

Figure 2. The count of crossings of the mean as a function of point intensity. The drop in the plot may be due to this being the optimal q for the specific point intensity (see text).

An important question to be answered with respect to this new term is if it will improve the precision of the GSE metric. However, an assessment must also be made to show how it influences the ability of the GSE metric in differentiating degrees of non-uniformity in spatial point patterns. Figure 3 exemplifies four different point distributions with different degrees of clustering (non-uniformity).

Figure 4a-d show the corresponding variation of the metrics GSE and GSE* for different point intensities n, in each case, as a function of number of quadrats, q. The graphs all have clusters of n_c = 5, but different σ (= 2, 5, and 8). As the non-uniformity approaches CSR, it is seen that the required q for optimal detection power decreases, i.e. the minimum peak of the curves is shifted towards smaller q's. As the patterns become more uniform for spatial distributions that approach CSR, a low q is thus necessary to detect non-uniformity. However, it is also apparent that most of the curves for the different degrees of non-uniformity separate as q increases. This means that the metric's ability to *differentiate* the different spatial distributions is higher for larger q's, as long as the non-uniformity is large enough to be detected.

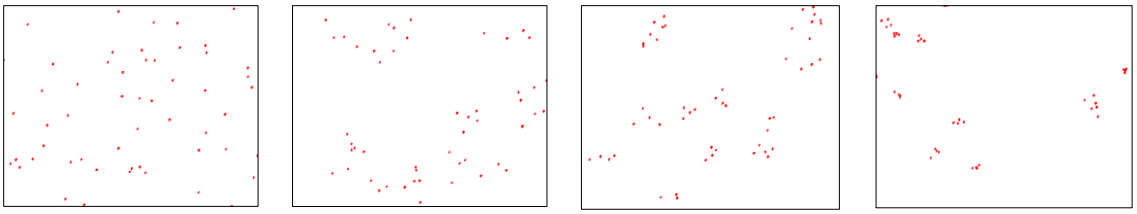

Figure 3. Examples of the spatial point distributions generated and tested in Figure 4, with a) CSR, b) sigma=8 c) sigma=5, and d) sigma=2.

It is suggested that the difficulty in detecting vague non-uniformity with higher *q*'s may be related to the problem of the relative localization of the quadrats, discussed in the previous section. The graphs of GSE* are indeed different, and seem to have a better detection power for larger *q*'s, compared to the original GSE. Moreover, the differences between the different degrees of non-uniformity are larger, suggesting a better ability to differentiate. The new expression does, however, seem to be unstable for lower *q*'s, indicating that larger *q*'s in this case leads to both better stability and resolution. To reveal how the GSE and GSE* may be used in practice, an experimental study will be presented in the next sections.

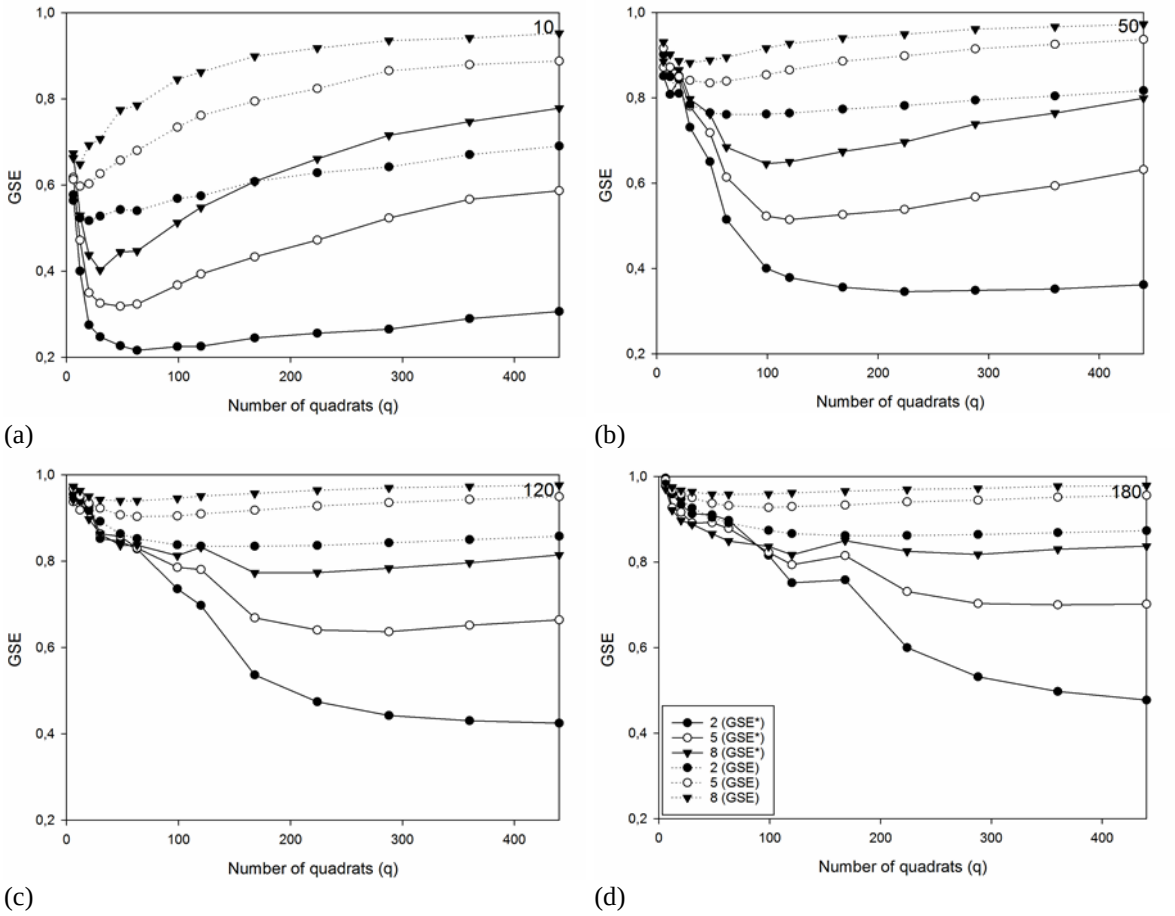

Figure 4. The effect of q on the deviation from CSR. The different graphs represent different degrees of clustering, with σ=2 being closest to CSR. a) n=10, b) n=50, c) n=120, d) n=180.

EXPERIMENTAL

Materials and Methods

Four alloys were DC-cast at Hydro Sunndalsøra, and samples were cut out of the billets at a distance of ~3-4 cm from the centre and ~2 cm from the edge. The chemical composition for this material is listed in Table 1. The samples were homogenised in an air furnace at a final holding temperature of 575ºC, for 2 hours and 15 minutes. Three different heating rates were used, and all samples were water quenched upon removal. The heating rate denoted "Normal" was chosen according to a typical industrial heating rate, using a five stage heating procedure set to an average of 4.6 ºC/min until reaching 525 ºC, and subsequently 1.0 ºC/min until reaching the final temperature. The "Slow" heating rate was chosen to be ½ · "Normal" (i.e. an average of 2.3°C/min from 25-525°C), while the "Fast" was set to 2 · "Normal". As a consequence of the different heating rates, the total amount of time in the furnace was different for each heating rate.

Samples were prepared by grinding and polishing for the microstructure investigation. Dispersoid characteristics were studied in a scanning electron microscope (SEM), Zeiss Ultra 55 LE. Back-scatter electron (BSE) imaging was used to obtain a Z-contrast and separate the Mn-dispersoids from the matrix. The acceleration voltage was set to 4 kV to minimize the penetration volume, and a working distance of 7.3 mm was found optimal for the BSE detector. 100 such images were taken of each alloy and heating rate and these were taken in a straight line through the samples, covering a distance of 1500 µm, and crossing approximately 18-22 grains. The total area covered was ~0.036 mm^2 for each sample.

The images were analyzed in the software IMT iSolution. Thresholding was carried out manually for each image, and the final result compared to each original image. Only dispersoids of sizes from 20-300 nm in diameter were accepted. Mathworks' software Matlab was used as the main tool in order to execute the different calculations in the evaluation of the GSE metric.

Table 1. Alloys investigated in this study. The compositions are shown in wt%, and are averages of 4 XRD scans of each billet.

Alloy	Si	Mg	Fe	Mn	Cr	Cu
6063	0.52	0.47	0.22	0.05	-	-
6005	0.59	0.55	0.19	0.14	-	0.11
6061	0.67	0.84	0.23	0.06	0.08	0.24
6082	1.03	0.66	0.21	0.51	-	-

Experimental Results: Number Density and Area Fraction of Dispersoids

Figure 5 shows results for the number density and % area of both alloys. Here, the "Slow" heating rate has been chosen as a reference, and the variation in dispersoid density is expressed as percent change with increasing heating rate. No significant differences was seen in the number density measurements for alloy 6063 when increasing the heating rate from "Slow" to "Normal", however, increasing to the "Fast" heating rate resulted in a ~30% drop in dispersoid density. A similar development was seen for the % area measurements. With increasing heating rates, the area covered by dispersoids was also found to decrease, but this time also between "Slow" and Normal". This behaviour of the % area is also found for alloy 6005, although less pronounced. However, for this alloy, the number density *increased* slightly with increasing heating rate. Due to the higher Mn content, both larger dispersoid densities and % areas are found in this alloy. Large variations in dispersoid density and % area between the images are also seen, expressed by the standard deviations, and indicating a non-uniform spatial distribution. The heating rate has more or less the same effect on the dispersoid density in alloys 6082 and 6005. However, in contrast, the % area of dispersoids in alloy 6082 remains more or less unchanged. The Cr content in alloy 6061 clearly made the dispersoid density less sensitive to differences in heating rate. The % area, however, decreased somewhat when increasing the heating rate from "Slow" to "Normal". Finally, by examining the % area plot, it may be

seen that the largest percent change with increasing heating rate is found for the leanest alloy, and the percent change decreases with increasing alloying content.

The results concerning the spatial distribution of dispersoids, in terms of the original GSE and the modified GSE*, are presented in Table 2. Different values for q and q*, referring to GSE and GSE*, respectively, were selected based on the discussion in Section 2. Q was set to correspond to q/n=1, and q* was chosen based on when the *number of crossings* in Figure 2 stabilizes. Both GSE and GSE* show a clear decrease with increasing heating rate for alloys 6063 and 6005, but the modified metric shows lower values than the original GSE. For 6061 and 6082 the trends are not clear. The GSE and GSE* for the 6061 alloy seem to decrease, but the trend is very weak. The same trend is, however, observed in the relative standard deviation, $s/\bar{x}$, showing the variation between the images, though also weak. Finally, 6082 shows no trend as the "Normal" heating rate resulted in the poorest spatial distribution.

In addition to the GSE and GSE* which return results about the spatial distribution *inside* the images, it may be useful to assess the variation in density *between* the images. A measure for this is the relative standard deviation, which increases with increasing non-uniformity, and is also found in Table 2. It corresponds quite well with the results from the GSE analysis, and is thus an independent metric that supports these results of the GSE and GSE*.

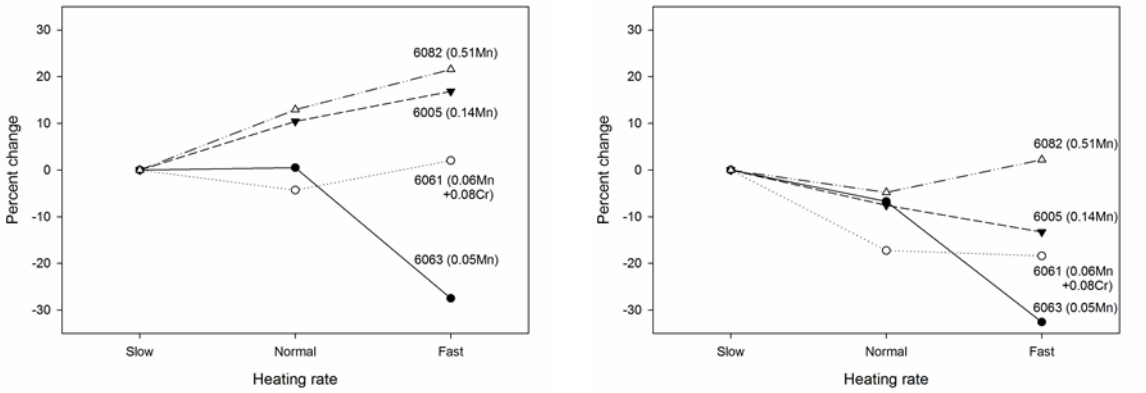

Figure 5. Percent change in dispersoid number density (a) and %area (b) as a function of heating rate.

Table 2. The results from the GSE analysis.

Alloy	Heating rate	n	q / q*	GSE	$s/\bar{x}$	GSE*
6063	Slow	1879	12/99	0.90	0.56	0.80
	Normal	1888	12/99	0.86	0.59	0.76
	Fast	1362	12/99	0.79	0.73	0.71
6005	Slow	4979	48/180	0.97	0.26	0.92
	Normal	5555	48/180	0.95	0.34	0.84
	Fast	5818	48/180	0.93	0.41	0.80
6061	Slow	12010	120/224	0.96	0.42	0.81
	Normal	11496	120/224	0.95	0.49	0.80
	Fast	12257	120/224	0.95	0.5	0.78
6082	Slow	18347	180/288	0.99	0.15	0.91
	Normal	20678	180/288	0.98	0.22	0.84
	Fast	22304	180/288	0.99	0.17	0.87

In Table 2 the trend seems to be the same for both the original and the modified GSE. In general, the GSE and the GSE* scores higher for slower heating rates, indicating a more uniform spatial distribution. According to Table 2, both the GSE and the GSE* decreases steadily with increasing heating rate for the two low-Mn alloys, 6063 and 6005. Moreover, the relative standard deviation of the density between the images is very high in each condition, and shows the same trend towards a more non-uniform spatial distribution for faster heating rates. The 6061 alloy seems to have a weaker trend than the above mentioned, and indicates that the higher precipitation temperature or slower diffusivity of the Cr-containing alloy makes the dispersoid density and spatial distribution less sensitive to changes in heating rate for the alloy compositions in question. The results from the 6082 alloy are more difficult to interpret, and are somewhat different for GSE and GSE*. There is no trend, but there is quite a big difference between the GSE and the GSE* results. GSE* seems to pick up some information the GSE does not.

DISCUSSION AND CONCLUSIONS

The main objective of the current study was to assess methods for evaluating the spatial distribution of dispersoids. Several methods have been developed, but many of these are not sufficiently precise or easy to implement. An attractive feature of the GSE is its simplicity. It only requires point coordinates or the count in each square of the grid, and the rest can be automated. The choice of using the quadrat-based method is based partly on convenience, but of course also on efficiency. The GSE proved to have the most efficient detection power in the studies by properties by Zhou et al. (2012) and Kam et al. (2013), but also gave indications of an ability to differentiate degrees of spatial uniformity. The latter was dismissed by Zhou et al. (2012) due to overlapping intensity distributions. However, these were only partially overlapping for the GSE, and could clearly be distinguished from each other. Zhou's conclusion was based on an interest in evaluating whether *one image* has a certain spatial distribution, and this is not a relevant concern in the present study. At high magnifications, such as those needed when studying dispersoids, both density and spatial distribution may vary significantly from image to image, and the main concern is thus whether a *sample population* of images differs from another.

Figure 6 shows how the GSE metric consistently picks up the differences in spatial distribution as the cluster parameters are gradually changed. This indicates that the GSE indeed *is* able to differentiate spatial uniformity of sample populations. However, the graph where only σ is changed shows that the ability to differentiate decreases as the spatial distribution approaches uniformity. This is also what was pointed out by Zhou et al. (2012), where the largest overlaps were seen close to CSR. However, the effect of each incremental change of σ on uniformity becomes smaller as σ increases. The behaviour of the graph is thus a result of the spatial distribution changing less, and is not caused by problems with the metric. Although this is true, it is also obvious that the necessity to differentiate spatial uniformity disappears as it approaches uniformity.

A problem appears, however, when the point intensity is large. This is seen in Table 2, where the GSE of 6082 is almost 1. By visual inspection of the relevant BSE micrographs (not included here), it is obvious that this cannot be accurate. The question is whether GSE* can improve the sensitivity of the metric. This effect was already seen in Figure 5, where the graphs are more spaced than for the GSE. Moreover, this is again expressed in Table 2 where GSE* shows the same trend as for the GSE, but with lower values. It also seems to pick up information in the analyses of 6061 and 6082 that GSE cannot. These results are, however, ambiguous.

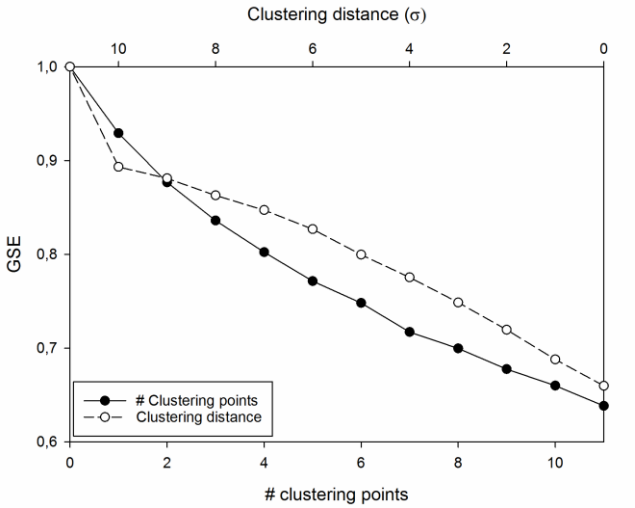

Figure 6. The variation of GSE with the number of clustering points (σ=constant) and the standard deviation of the distribution of clustering points (n_c = constant). Conditions close to CSR will only occur at $\sigma \gg 10$, leading to the discontinuity for the clustering distance graph at σ=10. In both cases q has been set constant to 6·8=48.

In Table 2 the trend seems to be the same for both the original and the modified GSE. In general, the GSE and the GSE* scores higher for slower heating rates, indicating a more uniform spatial distribution. Earlier studies have found the spatial distribution of both Cr- and Mn-containing alloys to be dependent on the heating rate (Lodgaard & Ryum, 2000b). In general, both a slower heating rate, and a lower homogenisation temperature seems to promote a more uniform spatial distribution (Lodgaard & Ryum, 2000a; Lodgaard & Ryum, 2000b). In Lodgaard & Ryum's study (2000a; 2000b; 2000c), Cr-containing alloys required a slower heating rate than the Mn-containing alloys, and the critical heating rates for a homogeneous spatial distribution were far above the one's used in the current study. However, the alloys used were also much denser, and this may have a significant effect. According to Table 2, both the GSE and the GSE* decreases steadily with increasing heating rate for the two low-Mn alloys, 6063 and 6005. Moreover, the relative standard deviation of the density between the images is very high in each condition, and shows the same trend towards a more non-uniform spatial distribution for faster heating rates. The 6061 alloy seems to have a weaker trend than the above mentioned, and indicates that the higher precipitation temperature or slower diffusivity of the Cr-containing alloy makes the dispersoid density and spatial distribution less sensitive to changes in heating rate for the alloy compositions in question. The results from the 6082 alloy are more difficult to interpret, and are somewhat different for GSE and GSE*. There is no trend, but there is quite a big difference between the GSE and the GSE* results. GSE* seems to pick up some information that the GSE does not.

To summarize it may concluded the Global Shannon Entropy (GSE) metric with a careful selection of relevant parameters, is an adequate metric for the detection of non-uniformity of dispersoid structures in Al-Mg-Si-alloys. Moreover with the new term it has been demonstrated that the ability to differentiate degrees of spatial uniformity has improved.

ACKNOWLEDGMENTS

This work has been supported through the BIA RolEx Project No. 219371 by Hydro Aluminium and the Research Council of Norway. The authors would like to thank Hydro Sunndalsøra for the material in this study, and especially Jostein Røyset and Oddvin Reiso for help in performing the homogenisation heat treatment and valuable discussions.

REFERENCES

Avrami, M. (1939). Kinetics of Phase Change. I General Theory *J. Chem. Phys.*, 7, 1103-1112.

Avrami, M. (1940). Kinetics of Phase Change. II Transformation Time Relations for Random Distribution of Nuclei *J. Chem. Phys.*, 8, 212-224.

Avrami, M. (1941). Granulation, Phase Change, and Microstructure Kinetics of Phase Change. III *J. Chem. Phys.*, 9, 177-184.

Bichel, H., Ried. A. & Langerweger, L. (1981). Metallographic investigation of the influence of small additions of manganese to AlMgSi0.5 alloys. *Aluminium*, 57, 787-789.

Bryant, A.J., Rise, E., Field, D.J., & Butler, E.P. (1989). Al-Mg-Si extrusion alloy and method. Alcan International, European Patent 0 222 479 B1, granted 1989.

Cressie, N. (1993). *Statistics for spatial data*. (John Wiley & Sons, Inc.).

Diggle, P.J. (2013). In *Statistical Analysis of Spatial and Spatio-Temporal Point Patterns, Third Edition*, (Chapman and Hall/CRC), 55-81.

Kam, K.M., Zeng, L., Zhou, Q., Tran, R. & Yang, J. (2013). On Assessing Spatial Uniformity of Particle Distributions in Quality Control of Manufacturing Processes. *J. Manuf. Syst.*, 32, 154-166.

Lodgaard, L. & Ryum, N. (2000a). Precipitation of dispersoids containing Mn and/or Cr in Al-Mg-Si alloys. *Mater. Sci. Eng. A*, 283, 144-152.

Lodgaard, L. & Ryum, N. (2000b). Precipitation of chromium containing dispersoids in Al-Mg-Si alloys. *Mater. Sci. Technol.*, 16, 599-604.

Lohne, O. & Dons, A.L. (1983). Quench sensitivity an AlMgSi-alloys containing Mn or Cr. *Scan. J. Metall.*, 12, 34-36.

Reiso, O. (2004). Extrusion of AlMgSi Alloys Proceedings of the 9th International Conference on Aluminium Alloys 32. Edited by J.F. Nie, A.J. Morton and B.C. Muddle © Institute of Materials Engineering Australasia Ltd, 32-46.

Sheppard, T. (1999). *Extrusion of aluminium alloys*. (Springer Science & Business Media).

Zhou, Q., Zeng, L., DeCicco, M., Li, X. & Zhou, S. (2012). A Comparative Study on Clustering Indices for Distribution Uniformity of Nanoparticles in Metal Matrix Nanocomposites. *CIRP J. Manuf. Sci. Technol.*, 5, 348-356.